Future Cities and Environment
ISSN 2363-9075 Volume 11 (2025)

https://doi.org/10.70917/fce-2025-036
Article

Performance Investigation on the Heat Transfer of Composite rGO-SiO_2 Nanofluid in a Radiator

Luke O. Ajuka [1] and, Christopher C. Enweremadu [2]

[1] Department of Mechanical, Bioresources and Biomedical Engineering, University of South Africa, ajukalo@unisa.ac.za
[2] Department of Mechanical, Bioresources and Biomedical Engineering, University of South Africa, enwercc@unisa.ac.za
* Corresponding author: ajukalo@unisa.ac.za

Abstract: High-performing cooling fluids are increasingly gaining prominence in thermal applications due to their superior heat transfer (HT) features compared to conventional coolants. This is attributed to the sub-optimal cooling and heat transfer limitations by conventional coolants. Reports reveal that HT enhancement includes different modifications to the radiator for effective heat dissipation, engineered suspensions of nanoparticles in base fluids ensures the direct deployment of existing radiators. In this study, reduced graphene oxide (rGO) nanoparticle was prepared by modified Hummer's technique via reduction process, with graphite powder as starting material, while silicon dioxide (SiO_2) was commercially sought. A comparative study was conducted to investigate the heat transfer of de-ionised (DI) water-based rGO-SiO_2 against its individual make-ups (rGO and SiO_2). At different volumetric concentrations (0.1%–0.3%) and temperature (20-60°C), SiO_2-rGO|0.3 composite nanofluid achieved a thermal conductivity (TC) enhancement of 16.8%, 9.4%, 7.1%, and 1.8% over the DI-Water, SiO_2|0.1, rGO|0.1, and SiO_2|0.3, which suggest a quick temperature equalization and better heat dissipation potential via Brownian motion, but 0.6% lower Tc compared to rGO|0.3 nanofluid. The viscosities of SiO_2|0.1, rGO|0.1, SiO_2|0.3, rGO|0.3 and SiO_2-rGO|0.3 nanofluids increased by 4.5%, 8.8%, 12.2%, 17.0%, and 14.0%, respectively, which may lead to an increase in pumping power demand, however, the positive figure of merit (TCR>1.0) justifies the nanofluids as better alternative to the basefluid. Furthermore, the Nu values of DI-Water/rGO SiO_2|0.3 was enhanced by 27.4%, 11.6%, 13.2%, 7.6% and 3.9% over the basefluid, SiO_2|0.1, rGO|0.1, SiO_2|0.3 and rGO|0.3 nanofluids, with an observable Nu increment of 3.71% and 8.87% of SiO|0.3 and rGO|0.3 compared to SiO|0.1 and rGO|0.1, respectively. In conclusion, TC ratio of the nanofluids were above unity, indicating enhanced heat transfer capability of the nanofluids compared to the base-fluid, and the MATLAB implementation of the proposed nusselt number correlation, fitted from experimental data achieved an R2 = 0.964.

Keywords: modified hummer's technique; hybrid nanofluid; heat transfer; thermal conductivity ratio; nusselt number correlation

1. Introduction

The enhancement of heat transfer performance in automotive and industrial cooling systems has attracted substantial attention over the past decades. In the context of thermal energy systems, particularly in heating, ventilation, and air conditioning (HVAC), the complementary roles of storage, transfer, and delivery of heat, aids adequate thermal management (Aydin et al., 2025; CUCE, 2025; Izzah et al, 2025), with specific applications in building heating systems (for hot water or steam), laboratory and research equipment (to regulate heat in calorimetry or thermodynamic experiments), spacecraft and satellite thermal management (for dissipating waste heat from electronics and on-board systems through radiative heat transfer, e.g., international space station uses deployable radiators and satellites use radiator panels to maintain thermal balance), electronics and data centres for cooling high-performance computers (e.g.,

gaming rigs, supercomputers), power generation plants for transformer cooling and generator cooling systems, railway and mass transit heating to heat passenger compartments in train coaches and metro systems, agricultural and animal housing heating to maintain thermal comfort in greenhouses, poultry farms, and livestock shelters, swimming pool heating systems to control water temperatures, and medical and pharmaceutical equipment to cool MRI, X-ray tubes, and CT scanners (Vadiee et al., 2020; Aacharya et al., 2023; Puttige et al., 2022).

Radiators, as critical components in thermal management systems, including systems such as hybrid, electric, fuel cell, industrial engines aerospace systems (Li et al., 2025; Dan et al., 2023; Gong C. et al, 2020, Yakubu et al., 2024, Madheswaran et al., 2022); require effective cooling fluids to ensure optimal performance and energy efficiency (Dika et al., 2025; Lipnicky et al., 2024). Traditional heat transfer fluids such as water, ethylene glycol, and their mixtures possess relatively low thermal conductivity, which limits their efficiency in high-performance applications (Bencs et al., 2021; Pacifique et al., 2023), and to address this limitation, nanofluids, which are fluids engineered by dispersing nanoparticles into base fluids are recently been deployed extensively due to their potential to significantly improve thermal conductivity and convective heat transfer rates (Porgara et al., 2024; Rahman et al., 2024). Among various nanoparticles, certain metal oxides such as SiO_2 have been widely employed due to their stability, low cost, and ease of preparation (Zango et al., 2025; Hashimoto et al., 2021). However, their relatively low thermal conductivity limits the maximum achievable enhancement (Hashimoto et al., 2021). In contrast, carbon-based materials, especially reduced graphene oxide (rGO), which exhibit extraordinary thermal conductivity and surface area, making them highly promising for thermal applications (Anegbe et al., 2024; Malavekar et al., 2024). On this basis, composite nanofluids, incorporating more than one type of nanoparticle in basefluid, have emerged as a strategy to synergize the desirable properties of different materials and achieve superior thermal performance (Haeri et al., 2024; Ali et al., 2018). Recent investigations suggest that hybrid nanofluids, particularly those combining graphene related composites, such as SiO_2, metal oxides, could offer significant improvements in heat transfer characteristics, yet their application in practical systems such as radiators remains underexplored.

Furthermore, reports shows that studies have been conducted to investigate the thermophysical properties of nanofluids originating from different allotropes of the interstellar carbon (10–25% polycyclic aromatic hydrocarbons (PAHs) thought to hold the explanation to the origin of life), perhaps, to infer the impact of the different structural properties on the heat transfer capacities (Yi et al., 2021), including fullerenes (Quadros et al., 2022; Reding et al., 2022), carbon nanotubes (Li et al., 2020; Khoswan et al., 2024), and graphene (Elsaida et al., 2021; Yusuf et al., 2025), among the 703 crystal structures in 121 of the 230 space groups of three-dimensional carbon allotropes that have been proposed based on SACADA (Samara Carbon Allotrope Database) statistics (Hoffmann et al., 2016). However, the attributed stability and reduced pressure drop capacity of rGO marks its uniqueness for use in nanofluids applications for example, Bahiraei and Heshmatian (2018) reported that it stabilizes and prevents sedimentation or aggregation of the nanofluids. Overall, this implies that there is a dearth in comprehensive reports of studies on the synergistic effects of combining hybridized composite nanoparticles' on overall thermo-physical properties, flow characteristics, and heat transfer rates under operable conditions. In an effort to bridge this gap, various studies have been conducted in this direction to proffer efficient and sustainable thermal management solutions, as highlighted in related studies below. Studies on the thermal properties of rGO-based nanofluids includes that of Sharma et al. (2024) which investigated the thermal conductivity of nanofluids containing graphene oxide (GO), functionalized GO (f-GO), and rGO. Their findings revealed that at a concentration of 0.23 wt.%, the thermal conductivity enhancements were 15.3% for GO, 21.8% for f-GO, and 11.9% for RGO compared to deionized water, and the superior performance of f-GO was attributed to increased interlayer coupling due to covalent and hydrogen bonding, which also contributed to better stability of the nanofluids.

In another study, Bharadwaj et al. (2024) examined rGO-based nanofluids and reported a maximum thermal conductivity enhancement of 27.5% at 0.15 vol% fraction and 60 °C. The study highlighted a linear relationship between thermal conductivity and temperature, and a polynomial relationship with concentration, emphasizing the potential of rGO nanofluids in solar applications. In addition, as desirable as the enhancement of thermal conductivity is, the need to balance the challenges of the accompanying increase in viscosity, such as higher pumping power requirements, for practical application of nanofluids has underscored the relevance and significance of related studies such as the viscosity study by Hadadian et al. (2014) on the viscosity of graphene oxide/ethylene glycol nanofluids, which reported an observed 3.4-fold increase in viscosity at a concentration of 0.005% and 20 °C. This significant rise in viscosity, even at low concentrations, underscores the need for careful optimization. Similarly, Cabaleiro et al. (2018) reported an increase in viscosity up to 130% for GO/water nanofluids at concentrations ranging from 0.0005 to 0.1%. These findings suggest that while nanoparticle addition enhances thermal properties, it also necessitates a trade-off with fluid dynamics. Additionally, on heat transfer (HT)

performance metrics, Ranjbarzadeh et al. (2017) investigated the convective heat transfer of water/graphene oxide nanofluids in a tube under air cross-flow. They reported an increase in the average Nusselt number by up to 51.4% at a concentration of 0.2%, indicating enhanced convective heat transfer performance. In another study, Bai et al. (2020) observed an increase in the Nusselt number ratio from 1.02 to 1.18 with increasing GO concentration, demonstrating the positive impact of GO on convective heat transfer. Finally, on hybrid nanofluids, mixtures of different nanoparticles have been explored to synergistically enhance thermal properties while mitigating drawbacks like increased viscosity, including the study by Kazemi et al. (2020) which comparatively studied the mono and hybrid nanofluids containing graphene and silica. Their results indicated that hybrid nanofluids exhibited better thermal conductivity enhancements than their mono counterparts. Specifically, the hybrid nanofluid showed a 27% increase in thermal conductivity at 1.0 vol.% concentration and 50 °C, highlighting the potential of combining graphene and SiO_2 for improved thermal performance. Consequently, all the studies above did not investigate the figure of merit (FOM) for which it permissible to clarify the trade-off of adopting nanofluid despite the increased pumping power requirement, including the SiO_2-based hybrid nanofluid. Furthermore, while some of these studies reveal that the integration of high thermal conductivity carbon-based nanomaterials with stable metal oxide particles holds great promise for next-generation heat transfer fluids, none among these studies have specifically conducted studies on the impact of rGO-SiO_2 nanofluid with emphasis on its operability-based figure of merit (FOM) and efficiency as radiator coolant.

Furthermore, application of related nanofluids include include the studies by Ponangi et al. (2021), which utilized ultra-low concentrated rGO nanofluid (0.002-0.006 vol. %) in a radiator, at 80 – 170, 210 – 270, and 40 ºC and 60 ºC of hot coolant Re, air Re, and inlet temperature of hot coolant, respectively. They reported a maximum increase of 100.5 % and 111% for the convective heat transfer coefficient and effectiveness with a reduction in friction factor, respectively, at 0.006 vol. % concentration. They concluded that rGO nano-coolant offers great scope for reducing the radiator size and increasing its performance. Ong et al. (2022) utilised EG/Water-SiO_2 nanocoolant in a car radiator to determine the thermal profile. They reported that the 15–25 nm, SiO_2 nanofluid exhibited enhanced heat transfer performance. They noted that the SiO_2 1 vol% showed took a shorter time to achieve and maintain at optimal working temperature compared to other samples, with submission that SiO_2 nanocoolant possesses slightly higher properties than the base fluid and conventional coolant. They concluded that the average heat transfer coefficient is directly proportional to the volume concentration of nanofluids and the heat transfer performance of the radiator increased with the inclusion of nanoparticles to the base fluid. Furthermore, the experimental and numerical studies by Joshi et al. (2024) using Graphene Amine based nano-coolant with varied coolant temperatures (50 °C–80 °C) and flow rates (3 l/min to 9 l/min), achieved an elevated Nusselt numbers, heat transfer coefficients and heat transfer rates, compared to EG/De-ionised water basefluid. They noted a 20% deviation in the theoretical and practical experiments. They concluded that a maximum heat transfer enhancement and heat transfer coefficient of 154.3 % and 83.1% (3209.52 W/m^2K), were achieved at 80 °C temperature and 9 l/min flow rate of by the Graphene Amine.

Consequent to the submissions above, investigating the performance of rGO-SiO_2 nanofluid in a radiator, will significantly contribute to the fundamental understanding of hybrid nanofluids, and also provide practical insights for enhancing cooling system efficiency in automotive and industrial applications, as it further bridges the current research gap on development of more efficient and sustainable thermal management technologies from synthesis to application.

2. Materials and Method

The various materials and test-rig for the experiment were prepared and tested. For the nanofluid preparation, Silicon oxide (SiO_2) was commercially sought, while rGO was synthesized from graphite powder (using Sodium nitrate, potassium permanganate, sulphuric acid, hydrogen peroxide and distilled water). The sequential process summary involved is given in Figure 1.

2.1. Modified Hummer's Method: rGO Preparation

Improved strategies of nanoparticle synthesis for sustainable environment and renewable energy have remained the foundation of recent processing of nanofluids (Behera et al., 2025; Abady et al., 2024), including the use of surfactants for stability (Cakmak et al., 2020). But, surfactant addition impacts the overall property of the nanofluid (Kaggwa et al., 2023; Wang et al., 2021; Shamsuddin et al., 2021), a case this study tried to avoid by not using surfactant. In this study, the starting material, commercially sought graphite powder 99.9 % (Alfa Aesar Co.) of 0.5g was chemically exfoliated using the modified Hummers via its addition to a continuously stirred mix of 27 ml and 3 ml concentrated sulphuric acid (H_2SO_4) and phosphoric acid (H_3PO_4), at 9:1 volume ratio, respectively. Then, potassium permanganate

($KMnO_4$) of 3g was measured and slowly added to the solution, with 4-hours of continuous stirring. 10 ml of hydrogen peroxide (H_2O_2) was gradually added to the resulting darkish-green solution to eliminate excess of KMnO4 within 1hour of continuous stirring, and the solution of the ensuing exothermic reaction was cooled. Both hydrochloric acid (HCl) and deionized (DI) water of 10 ml and 30ml were respectively added, and the obtained solution was centrifuged at 5000 rpm for 10 minutes. The supernatant layer was decanted while the residuals was re-washed thrice with HCl and DI water to obtain the GO sample, which was heated at 300°C of 5°C min^{-1} for 2hours to produce the exfoliated reduced graphene oxide (rGO).

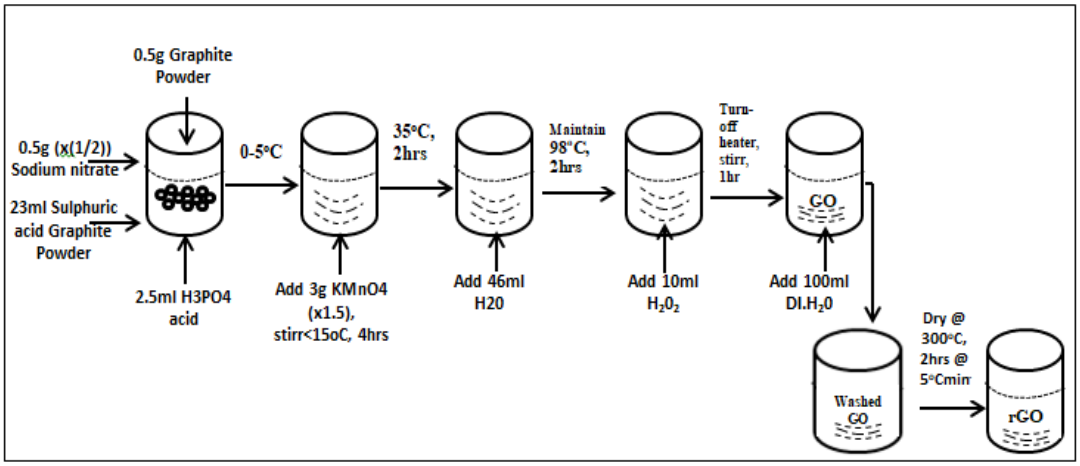

Figure 1. Summary of rGO Synthesis Process.

The water based mono SiO_2, rGO, and hybrid composite of rGO-SiO_2 samples were prepared via dispersion at a different volume concentrations (0.1% and 0.3%). The various water based fluids were ultrasonicated for 12-hours, and it was visually confirmed that there were no particle agglomeration and sedimentation. These nanofluids were prepared before the experimental application, in the next phase, and the material specifications used in the set-up are highlighted in Table 1.

Table 1. Material List and Technical Specification.

S/N	Measurement Device	Range	Specification / Uncertainty
1	Flow Meter	2 – 40L/min	Standard Analogue / ±0.17 L/min
2	Thermocouple	-50 – 750 °C	Type K / ±0.035°C
3	Pressure Gauge	1 – 1931kPa	Bourdon tube/ ±0.24kPa
4	Boiling Ring	220 -240V	1500W
5	Water Pump		0.373kW, 2.1A, 50Hz, (Maximum flow:
6	Pipes, clips and hoses		40l/m)
7	Frame fabrication		Materials: Plastic, metal and flexible rubber
8	Electrical wires and extension outlets		Mild steel frame 10A, 220V, 50/60Hz
9	Honda Radiator (Down-flow radiator)		1litre

The developed test rig (Figure 2), comprised of a reservoir, circulation, and measurement components in a closed-loop fluid system, assembled on a mobile steel frame for portability and experimental flexibility.

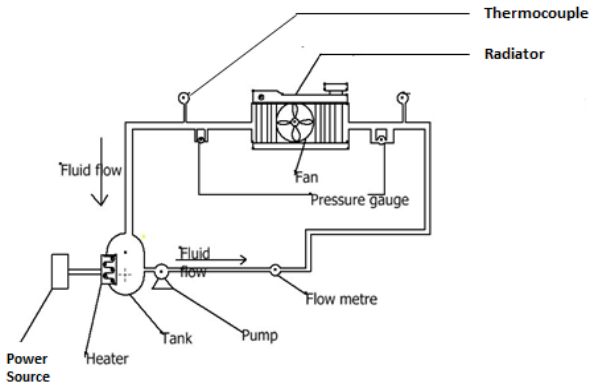

(a)

(b)

Figure 2. Experimental Set-up: (a) Schematic view; (b) Pictorial view.

The test-rig components include a single-row Aluminum core, tube and fin, radiator with cooling fan, 25-liter high-density polyethylene (HDPE) container served as the primary fluid reservoir, centrifugal pump (0.5 hp, 5-35L/min., and 220v (A/C)), and piping network (¾-inch and 1-inch PVC pipes, elbows, unions, and T-joints) for fluid transport to simulate typical industrial piping configurations, as well as Gate valves for flow regulation and section isolation. Valves were integrated into the circuit to control fluid flow, and hose clamps were used to ensure leak-tight connections of the reinforced flexible tubing utilised at critical junctions for easy dismantling and vibration-isolation. All these measuring instruments provide real-time data on the fluid dynamics during experimentation. Detail specification of the radiator is given in Table 2.

Table 2. Specifications of Radiator.

S/N	Parameter	Value (mm)
1	Tube numbers	34
2	Radiator length	371
3	Width of Radiator	527
4	Width of the radiator tube	37.5
5	Length of Tube	355
6	Length of Fin	9

7	Thickness of Fin	0.0008
8	Distance between adjacent fins	14

At different volumetric fractions, the tank receives the nanofluids. The pump is switched off to allow the nanofluid sample inside the tank to heat up and reach the intended temperature for the test (for example, 50 ºC). Once this maximum temperature has been reached, the pump is switched on and the nanofluid sample is able to be pumped into the radiator. The fluid exiting the radiator flows back to the storage tank, for the cycle to repeat itself, and records of the process parameters (temperature, pressure, flow-rate, etc.) are taken at intervals in order to analyse the fluid flow characteristics.

2.2. Uncertainty Analysis

For this study, the uncertainty analysis was conducted by determining the measurements' error. Errors in the measurement of volume flow rate and hydraulic diameter of the tubes are responsible for the uncertainty range of both Reynolds number and Nusselt number (Nu), and errors in the measurement of temperatures additionally affect Nu. According to Moffat's (1988) diffusion theory, equation 1 was used to estimate the uncertainty in the equipment measurements as shown in Table 1.0. Further runs were conducted to verify the reproducibility of the experiment.

$$U_R = \left[\sum_i^n \left(\frac{\partial R}{\partial V_i} U_{V_i}\right)\right]^{\frac{1}{2}} \tag{1}$$

2.3. Experimental Equations

The thermal properties of the samples, base fluids, mono, and hybrid nanofluids were first determined, for example, temperatures (using thermocouples), and substituted to obtain various thermal properties. Volume fraction:

$$\emptyset_{hnf} = \frac{\left(^{w}/_{\rho}\right)_i + \left(^{w}/_{\rho}\right)_j}{\left(^{w}/_{\rho}\right)_i + \left(^{w}/_{\rho}\right)_j + \left(^{w}/_{\rho}\right)_{bf}} \tag{2}$$

Density:

$$\rho_{hnf} = \rho_i \emptyset_i + \rho_j \emptyset_j + (1 - \emptyset_{hnf})\rho_{DW} \tag{3}$$

Specific heat capacity: Thermal equilibrium based model,

$$C_{p,mnf} = \frac{\emptyset\left(\rho C_p\right)_n + (1 - \emptyset)\left(\rho C_p\right)_{bf}}{\emptyset\rho_n + (1 - \emptyset)\rho_{bf}} \tag{4}$$

$$C_{p,hnf} = \rho_i \emptyset_i C_{p,i} + \rho_j \emptyset_j C_{p,j} + (1 - \emptyset_{hnf})\rho_{dw} \tag{5}$$

For the equations above Ø, ṁ, ρ, Cp are the volume fraction, mass, density, specific heat capacity of the fluids.

$$K_{mnf} = K_{bf}\frac{K_{np} + 2K_{bf} - 2\emptyset\left(K_{bf} - K_{np}\right)}{K_{np} + 2K_{bf} + \emptyset\left(K_{bf} - K_{np}\right)} \tag{6}$$

$$K_{hnf} = K_{bf}\left(\frac{\frac{\left(\emptyset_{npi}K_{npi} + \emptyset_{npj}K_{npj}\right)}{\emptyset_{i,j}} + 2K_{bf} + 2\left(\emptyset_{npi}K_{npi} + \emptyset_{npj}K_{npj}\right) - 2\emptyset_{i,jK_{bf}}}{\frac{\left(\emptyset_{npi}K_{npi} + \emptyset_{npj}K_{npj}\right)}{\emptyset_{i,j}} + 2K_{bf} - \left(\emptyset_{npi}K_{npi} + \emptyset_{npj}K_{npj}\right) + \emptyset_{i,jK_{bf}}}\right) \tag{7}$$

In addition, the newton's cooling relation is utilized to determine the Nusselt number (Nu) and coefficient of heat transfer (h) as follows;

Heat transfer coefficient:

$$Q = hA_s(T_b - T_S) \tag{8}$$

Bulk Temperature:

$$T_b = \frac{T_{in} + T_{out}}{2} \tag{9}$$

Tube wall temperature:

$$T_s = \frac{T_1 + T_2 + \cdots . + T_8}{8} \tag{10}$$

Heat transfer rate:

$$Q = \dot{m} C_p \Delta T = \dot{m} C_p (T_{in} - T_{out}) \tag{11}$$

where, mass flow rate: $\dot{m} = \rho \dot{V}$
Substituting equation (11) into (8), and re-arranging;
Heat transfer coefficient (h):

$$h_{exp} = \frac{m C_p (T_{in} - T_{out})}{A_s (T_b - T_s)} \tag{12}$$

Propagated relative uncertainty in h:

$$\frac{\delta h}{h} = \sqrt{\left(\frac{\delta \dot{m}}{\dot{m}}\right)^2 + \left(\frac{\delta C_P}{C_P}\right)^2 + \left(\frac{\delta (T_{in} - T_{out})}{(T_{in} - T_{out})}\right)^2 + \left(\frac{\delta A_s}{A_s}\right)^2 + \left(\frac{\delta (T_b - T_s)}{(T_b - T_s)}\right)^2} \tag{13}$$

Reynolds Number (Re):

$$Re_{exp} = \frac{\rho \times V \times D}{\mu} \tag{14}$$

Uncertainty in Re is dependent on $\rho, V, D, and\ \mu$, as:

$$Re_{exp} = \frac{\rho \times V \times D}{\mu} = \frac{\rho D}{\mu} \times \frac{Q}{N_{tubes} A}$$

Re Uncertainty is computed as:

$$\frac{\delta Re}{Re} = \sqrt{\left(\frac{\delta Q}{Q}\right)^2 + \left(\frac{\delta \rho}{\rho}\right)^2 + \left(\frac{\delta \mu}{\mu}\right)^2} \tag{15}$$

Nusselt number (Nu):

$$N_u = \frac{E_{conv}}{E_{cond}} = \frac{h_{exp} \times D_h}{k} \tag{16}$$

Relative uncertainty in Nu:

$$\frac{\delta Nu}{Nu} = \sqrt{\left(\frac{\delta h_{exp}}{h_{exp}}\right)^2 + \left(\frac{\delta D_h}{D_h}\right)^2 + \left(\frac{\delta k}{k}\right)^2} \tag{17}$$

Where the hydraulic diameter:

$$D_h = \frac{4 \times A}{P}$$

The pumping power requirement by nanofluids necessitates the need for a figure of merit (FOM);
Thermal Conductivity Ratio:

$$TCR = \frac{K_{nf}}{K_{bf}} \tag{18}$$

Note: h, A_s, T_b, T_s, K, V, D, E_{conv}, E_{cond} are the heat transfer coefficient, surface area, bulk temperature, tube-wall surface temperature, thermal conductivity, velocity, internal diameter, thermal energy exchanged by convection and conduction, respectively. Subscript i and j represents SiO_2 and rGO; SiO_2-rGO = i, j nanoparticles; while T_i and T_o are inlet and outlet temperatures, and subscripts mnf and hnf are mono and hybrid nanofluids, respectively.

3. Result and Discussion

The results in terms of thermos-physical properties, heat transfer coefficient, figure of merit in relation to pumping power is elucidated in this section.

3.1. Hybrid Composite Characterisation

Particle morphologies were observed by scanning electron microscopy (SEM) model Jeol JSM-6010LV at a magnification of 1000× using a 15 kV accelerating voltage under Backscattered Electron Detector (BSD FULL) mode. The SEM image of rGO sheets reveals a disordered, crumpled-sheet-like morphology characteristic of rGO nanosheets. The bright regions represent agglomerated rGO flakes or clusters, whereas the darker areas are indicative of the porous structure and interstitial voids between sheets. This irregular texture, marked by overlapping and entangled lamellar structures, is a strong indication of the successful chemical reduction of graphene oxide (GO), where oxygen-containing functional groups are partially removed, leading to restacking and folding of the graphene sheets due to van der Waals attractions. The lateral size of the visible rGO flakes is observed within ~100 nm (Figure 3), which aligns with expectations for chemically synthesized graphene derivatives. The presence of voids and wrinkled textures provides evidence of high surface area and structural defects, both of which are beneficial for applications such as energy storage, catalysis, and thermal transport.

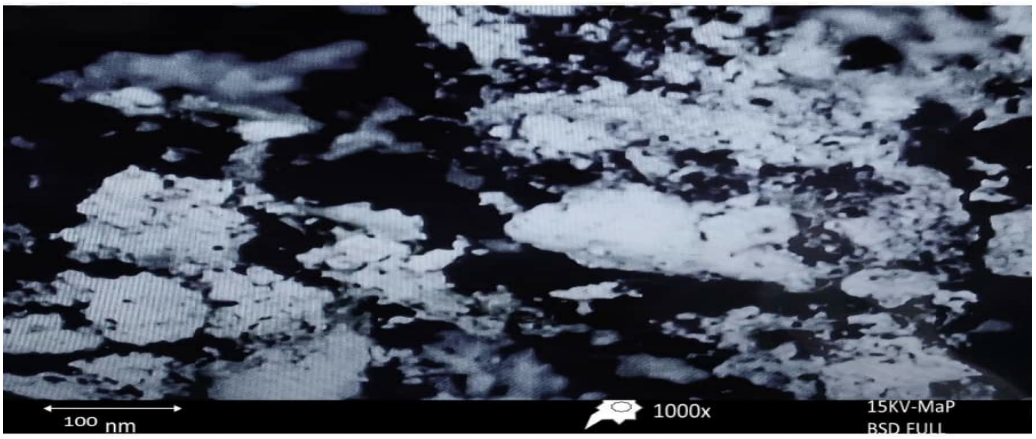

Figure 3. SEM Image of synthesized rGO.

Notably, the rough and uneven topography also implies potential interfacial compatibility, of multi-layered rGO structures with retained structural defects and wrinkles. Such features are critical for facilitating electron transport and anchoring nanoparticles or other functional agents in hybrid systems. The nanoscale thickness and irregular shape of the flakes further enhance the surface-to-volume ratio, a parameter crucial for adsorption, sensing, and catalytic applications.

3.2. Thermal Properties

The thermal properties (viscosity and thermal conductivity) of the base fluid and nanofluid samples at different temperatures range of are analysed in the given range 20 °C to 60 °C.

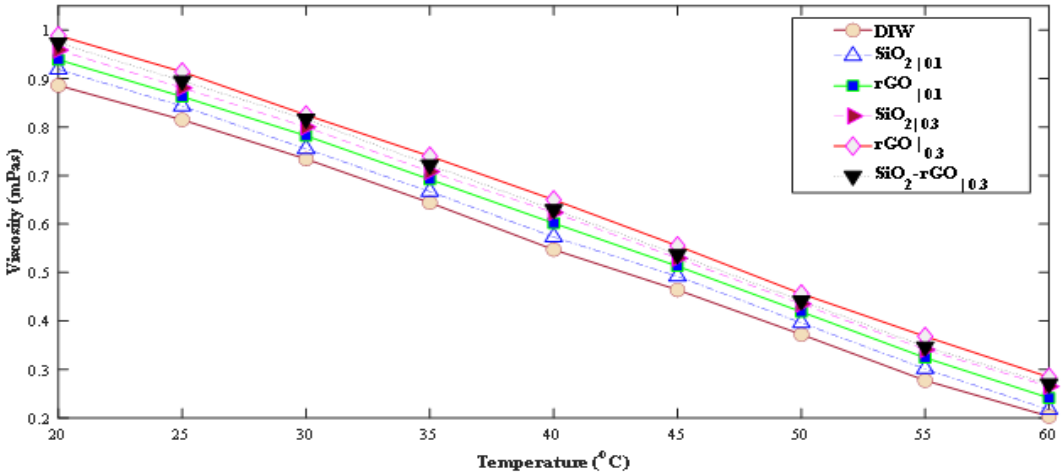

Figure 4. Viscosity of the basefluid and different nanofluid samples.

In Figure 4, which illustrates the plot of the different viscosities of the experimental samples against temperature, observation reveals that the basefluid and rGO|0.3 were the least and most viscous of the sample set, and viscosity decreased with increase in temperature. The basefluid viscosity is lower than the SiO_2|0.1, rGO|0.1, SiO_2|0.3, rGO|0.3 and SiO_2-rGO|0.3 nanofluids by 4.5%, 8.8%, 12.2%, 17.0%, and 14.0%. Further observation reveals that SiO_2-RGO|0.3 is less viscous than rGO|0.3 nanofluid, which implies a better flow and mixing potential.

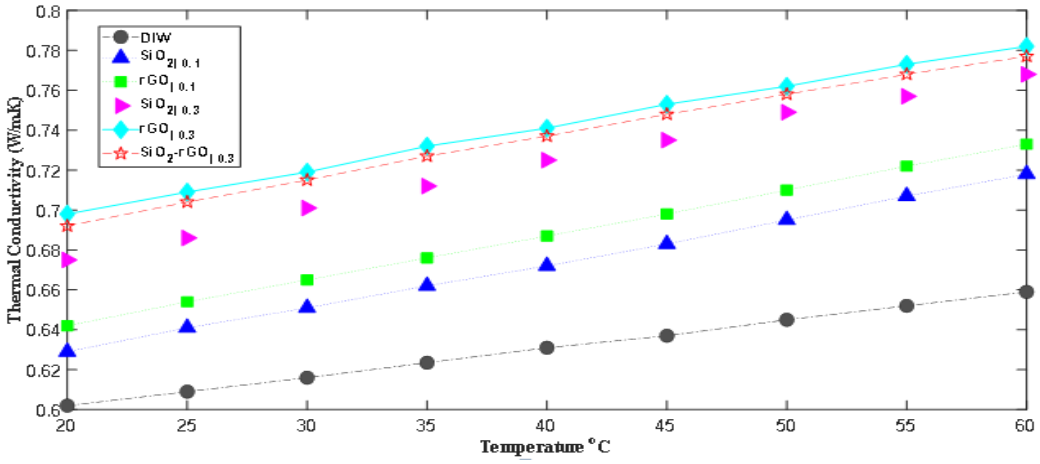

Figure 5. Thermal conductivity of the samples at different temperatures.

The impact of temperature on the thermal conductivity (TC) of the basefluid and nanofluids are illustrated in Figure 5. Observation shows that the DI water and rGO|0.3 had the least and highest TCs, with an increase in the TCs of all the fluids as temperature increases. The TC enhancement of the $SiO_{2|0.1}$, $rGO_{|0.1}$, $SiO_{2|0.3}$, $rGO_{|0.3}$ and SiO_2-$RGO_{|0.3}$ nanofluids were 6.7%, 9.03%, 14.7%, 17.5% and 16.8%, respectively. In addition, $rGO_{|0.3}$ had a higher TC of 0.64% over the SiO_2-$RGO_{|0.3}$ nanofluid.

3.3. Figure of Merit (FOM) and Enhancement

The thermal conductivity ratio (TCR) for the water based SiO_2|0.1, rGO|0.1, SiO_2|0.3, rGO|0.3 and SiO_2-rGO|0.3 were evaluated for how much they measure as alternatives. To be considered as better alternatives to the basefluid, TCR > 1 is a practical measure to ensure better heat transfer characteristics.

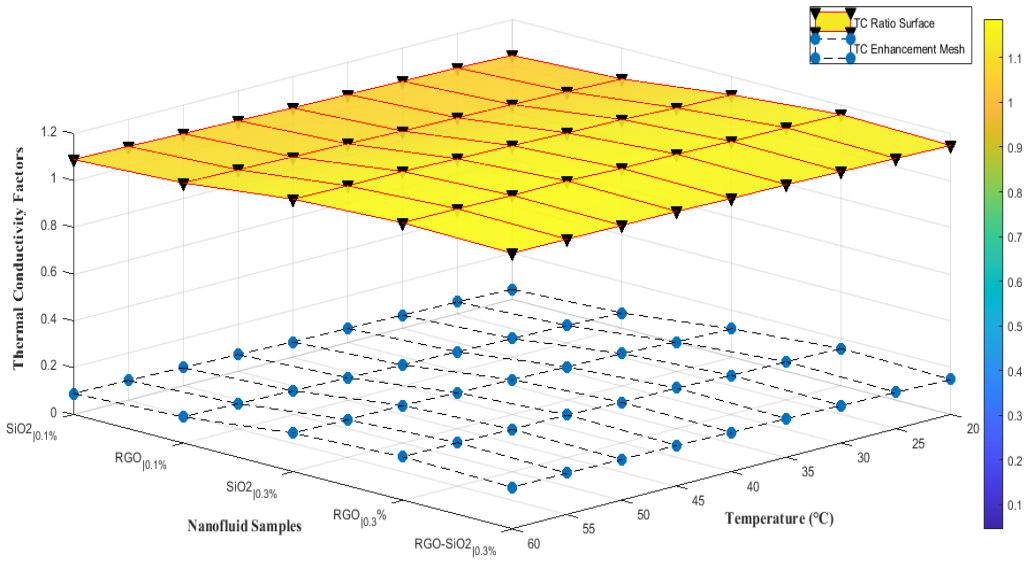

Figure 6. Combined surface plot of TCR and TCE over Temperature.

Figure 6 illustrates the thermal conductivity ratio (TCR) and thermal conductivity enhancement (TCE) of the experimental samples as a function of temperature. The average values of the TCR (yellow surface plot) are 1.07, 1.08, 1.15, 1.175 and 1.167 for SiO_2|0.1, rGO|0.1, SiO_2|0.3, rGO|0.3 and SiO_2-RGO|0.3, respectively. Each of this values are above unity (>1), indicating that they are better alternatives to the basefluid, for example, the higher the Mo value (Mo > 1), the better will be its heat transfer characteristics, despite being more viscous. rGO|0.3 has the highest TCR with the elevation being more pronounced at 60ºC. Additionally, the mesh plot shows the distribution of the TCE of the sample set. While the average TCE's of SiO_2|0.1, rGO|0.1, SiO_2|0.3, rGO|0.3 and SiO_2-RGO|0.3 are 6.7%, 8.9%, 17.5% and 16.7%, respectively; $rGO_{|0.3}$ has the highest TCE at 60ºC, which is 4.33% higher than SiO_2-RGO|0.3 nanofluid.

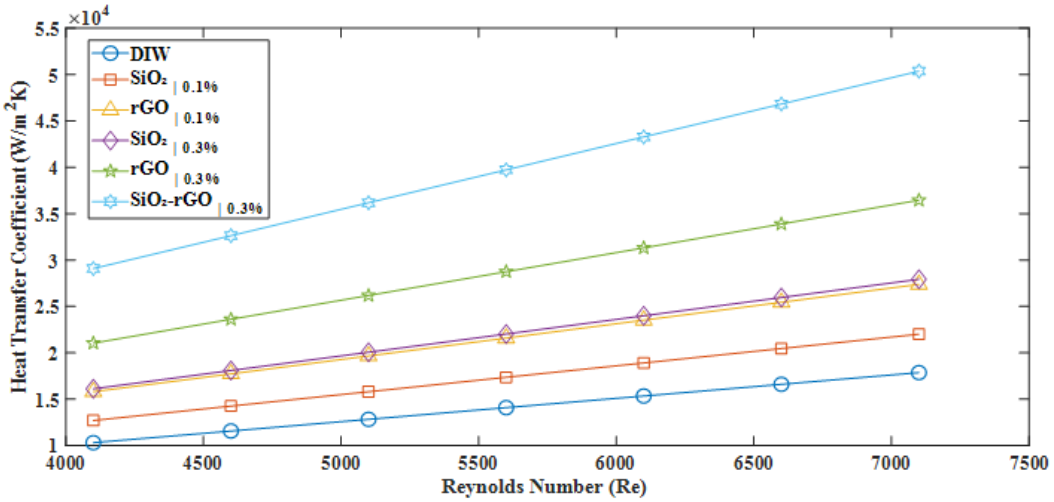

Figure 7. Heat transfer coefficient (h) of samples at different Reynolds number (Re).

The Figure 7 reveals the heat transfer coefficient of the samples (base fluid and nanofluids) at varying Re values. The nanofluids, $SiO_2|_{0.1\%}$, $rGO_{|0.1\%}$, $SiO_2|_{0.3\%}$, $rGO|_{0.3\%}$ and SiO_2-$rGO|_{0.3\%}$, were 23.2%, 53.22%, 56.3%, 104.0% and 121.8% higher over the basefluid. Within the Re range of 4100 to 7100, the figure shows a slight increase in heat transfer at Re 4100 to 4600, thereby implying slight heat transfer rate per unit area over time. Overall, the increased heat transfer coefficient is an indication of an enhanced mixing, and increased rate of heat transport within the fluid. SiO_2-$rGO|_{0.3\%}$, had the highest heat transfer coefficient.

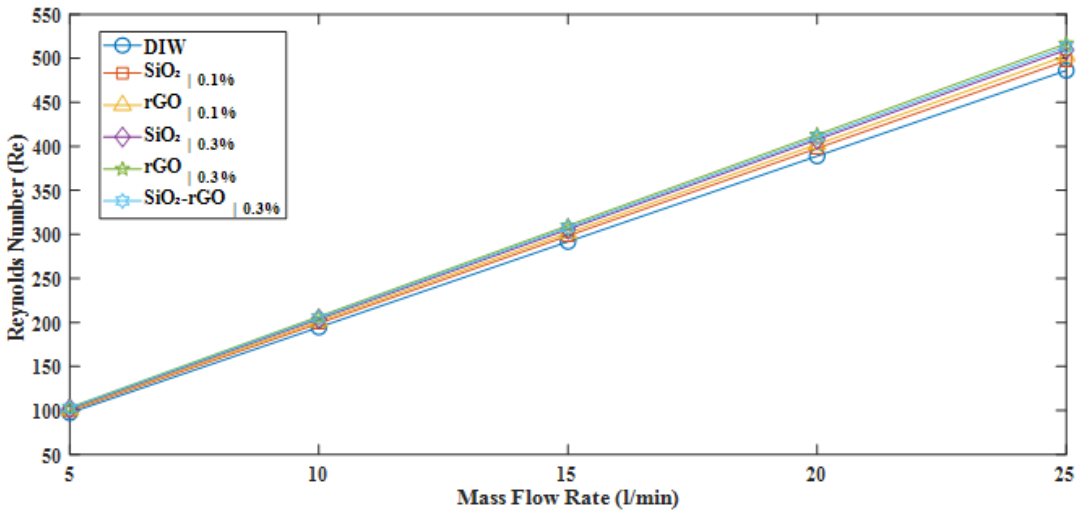

Figure 8. Impact of mass flow rate (ṁ) on Reynolds number (Re).

Figure 8 illustrates the influence of mass flow rate on Reynolds number (Re), with rGO|0.3% and DI water samples having the highest and the least Re. Furthermore, the highest and least Re values were achieved at mass flow rates of 25 l/min and 5 l/min. The result shows that increase in volume fraction increased the Reynolds number for both mono nanofluids.

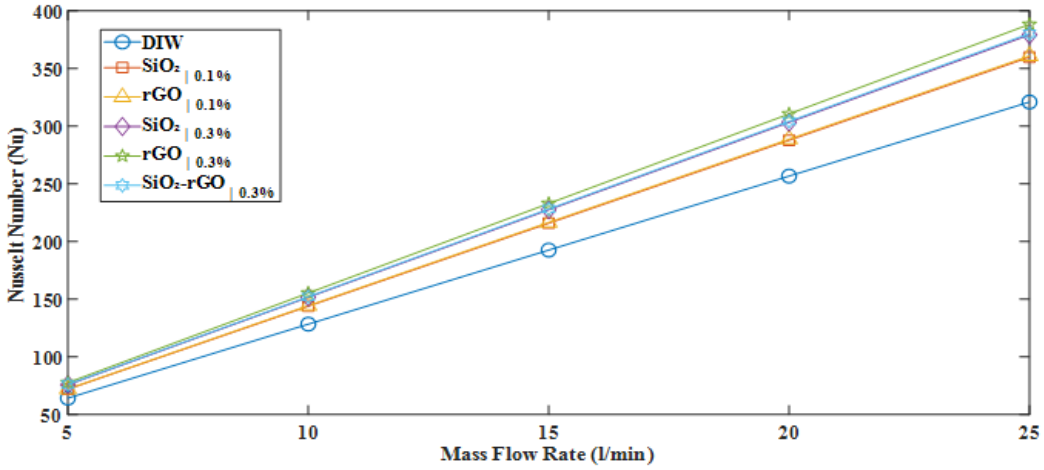

Figure 9. Impact of mass flow rate (ṁ) on Nusselt number.

Figure 9 shows the impact of mass flowrate on Nusselt number (Nu), observation shows that increase in mass flow rate (m) leads to increase in Nu, with a record of the least and the highest Nu being obtained at 5 l/min and 25 l/min. For all the samples, result shows that at different mass flow rate, RGO|0.3 has the highest Nu, in contrast to DI water with the least Nu. The result shows that increase in volume fraction increased the Nusselt number for both mono nanofluids.

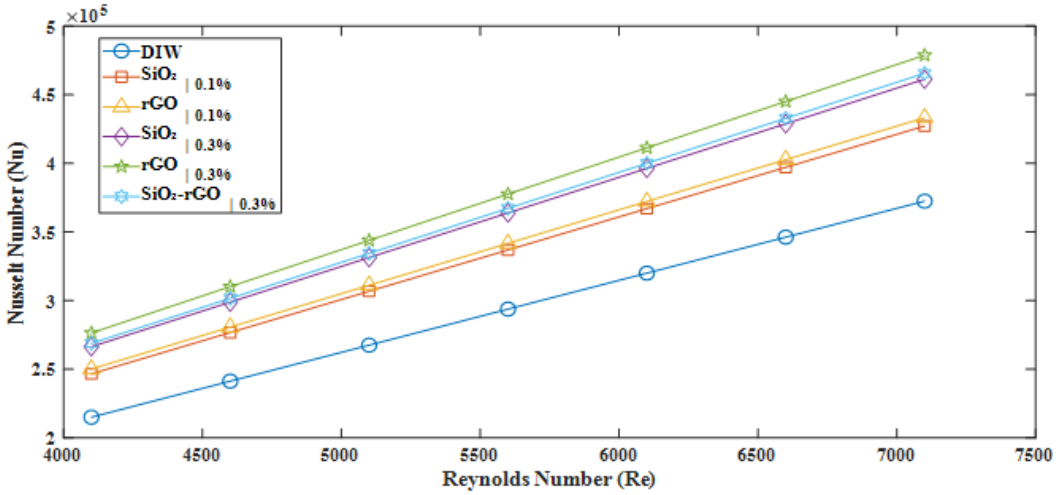

Figure 10. Nusselt number (Nu) of samples at different Reynolds number (Re).

The Figure 10 illustrates the relationship of Nusselt numbers of the experimental samples at varying Reynolds number. Statistical observation shows that the maximum deviation of the rGO|0.3% samples is 28.5% higher than the basefluid. Meanwhile, $SiO_2|_{0.1\,\%}$, $rGO|_{0.1\,\%}$, $SiO_2|_{0.3\,\%}$, and SiO_2-$rGO|_{0.3\,\%}$, were 14.7%, 16.3%, 23.8, and 25.0%, respectively. Furthermore, visual inspection reveals that Nu increased with Reynolds number, with the nanofluids exhibiting higher Nu values. This may be attributed to the enhanced heat transfer performance resulting from the increased thermal conductivity of the nanofluid which allows for a more efficient heat transfer. The increasing Nu value with increasing Re indicates increment in mixing and heat transfer rates, as well as turbulent flow potential, which is led by rGO|0.3% sample. This may result from the thinning of the thermal boundary layer at higher Reynolds numbers, which enhances the convective heat transfer process.

3.4. Propagation of Uncertainties

The uncertainties determined for the Reynolds number, heat transfer coefficient and Nusselt number based on experiment are summarized in Table 3.

Table 3. Uncertainties in h, Re and Nu.

Q (L/min)	δh (%)	δRe (%)	δNu (%)
5	% 3.63%	$\pm$ 3.40%	$\pm$ 3.76%
15	% 1.70%	$\pm$ 1.14%	$\pm$ 1.97%
25	% 1.43%	$\pm$ 0.69%	$\pm$ 1.75%

According to Table 3, it may be inferred that at low flow rate (5 L/min) uncertainties are noticeably larger, whereas, at 15–25 L/min they fall to around 1–2%. The **Re uncertainty falls with flow, resulting from the** flow meter's uncertainty value (±0.17 L/min). Furthermore, the relationship of Q, which grows wtih the fractional error (0.17/Q), which shrinks, may influence the δRe% drop from ~3.4% at 5 L/min to ~0.69% at 25 L/min. **Heat-transfer uncertainty (δh) and Nusselt uncertainty (δNu) follow the same trend, and as the h and Nu depend** on multiple measured quantities (temperatures, area, Cp, k), additional independent uncertainty contributions remain even when flow uncertainty is small, making them **slightly larger than δRe**.

3.5. *Regression* Fitting for Nusselt Number (Nu)

Using least square regression method, which was implemented in MATLAB, the average Nusselt number correlation was obtained based on the experimental data, and this is given in the equation [17];

$$\ln(N_u) = 0.4292\ln(Re^2) + 0.0201\ln(\emptyset\mu) - 0.4937\ln(\mu) - 0.04301\ln(Pr^2) \qquad (17)$$

This is valid for $0 \leq \emptyset \leq 0.3\%$

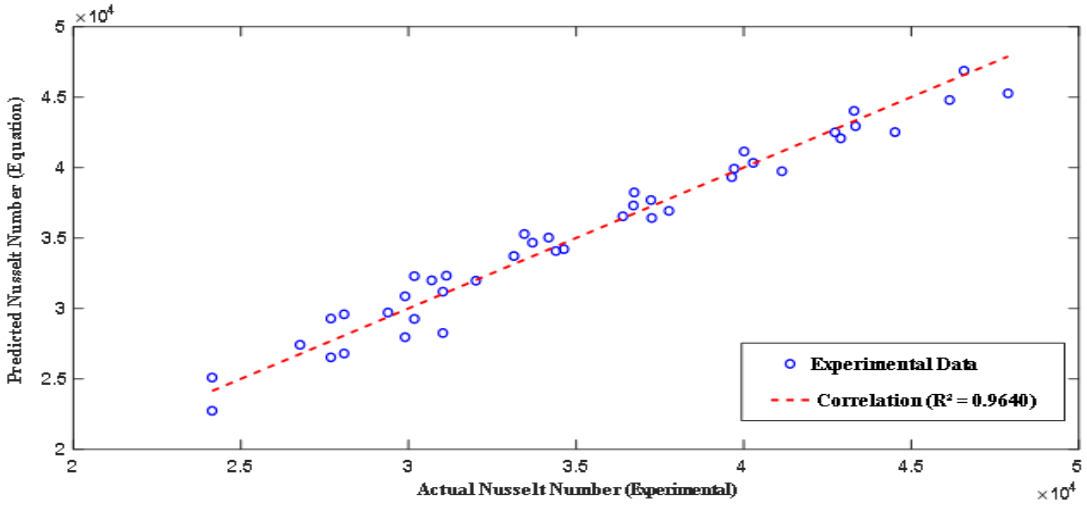

Figure 11. Proposed equation showing predictive correlation on experimental data

According to Figure 11, which compared the predicted and the actual Nu value, Points close to the red dashed line indicate a goodness of fit of the model. Observation reveals that **R^2** (= 0.9640) which quantifies how well the regression model explains the variability in the data is within $0.95 < R^2 < 1.0$, which is of a high predictive capability.

4. Conclusion

This study investigated the thermo-physical and heat transfer performance of various nanofluids, including mono and hybrid composition of SiO_2, rGO, and SiO_2–rGO nanoparticles dispersed in deionized water. The SEM morphological analysis of the synthesized rGO particle showed aggregated and wrinkled sheet-like structure. Viscosity measurements revealed that all nanofluids exhibited a decreasing trend with increasing temperature, with rGO|0.3 exhibiting the highest viscosity, while the basefluid remained the least viscous. Notably, the SiO_2–rGO|0.3 nanofluid showed improved flow-capability compared to rGO|0.3, indicating better mixing potential. Thermal conductivity enhancements were observed across all nanofluids, increasing with temperature. rGO|0.3 nanofluid exhibited the highest thermal conductivity enhancement (17.5%), slightly outperforming the SiO_2–rGO|0.3 hybrid nanofluid. The thermal conductivity ratio (TCR) and enhancement (TCE) also exceeded unity for all nanofluids, confirming their thermal performance superiority over the basefluid. The highest TCR and TCE were recorded at elevated temperatures, with rGO|0.3 exhibiting peak values. Heat transfer coefficients across the Reynolds number range (4100–7100) indicated significant enhancements, particularly for the SiO_2–rGO|0.3 nanofluid, which achieved a 121.8% improvement over the basefluid. The influence of mass flow rate on Reynolds and Nusselt numbers demonstrated that higher flow rates led to increased convective heat transfer. rGO|0.3 consistently exhibited the highest Nusselt numbers across flow conditions, while the basefluid remained the lowest. A regression-based Nusselt number correlation was developed using the least squares method, achieving a strong predictive accuracy with R^2 values between 0.95 and 1.0. This correlation effectively predicted relationship between flow dynamics and fluid properties within the tested volume fraction range (0–0.3%).

Overall, the findings affirm that rGO-based and hybrid nanofluids significantly enhance heat transfer performance, with SiO_2–rGO hybrids offering a beneficial compromise between thermal conductivity and viscosity. These results underscore the potential application of such nanofluids in advanced thermal management systems, particularly where efficient heat transport and stability are critical.

References

D. Aydin, H. Jarimi, B. Yuksel, Z. Utlu, S. Riffat, "Experimental Investigation of a Vertical Flow Moving Bed Thermochemical Heat Storage," Energy Catalyst, vol. 1, pp. 68–78, 2025. https://doi.org/10.61552/EC.2025.005

P.M. CUCE (2025), "Evaporative Cooling Technologies: From Past to Present," Journal of Global Decarbonisation, vol. 2025, no. 1, pp. 1–40., 2025. https://doi.org/10.17184/EAC.9493

F.N. Izzah, B.F.T. Kiono, K. Rozi, "Energy and exergy analysis of the XYZ ultra-supercritical steam power plant," Green Technology & Innovation, vol. 1, no. 1, pp. 8099, 2025. https://doi.org/10.36922/GTI.8099

Vadiee, A. Dodoo, E. Jalilzadehazhari, “Heat Supply Comparison in a Single-Family House with Radiator and Floor Heating Systems,” Buildings, vol. 10, no. 5, pp 1-22, 2020. https://doi:10.3390/buildings10010005

Aacharya, R. Koirala, S. Khanal, B. Baral, "Comparative analysis of radiant and radiator heating system for a residential building," IOP Conference Series: Materials Science and Engineering, vol. 1279, no. 1, pp. 012001. 2023. https://doi.org/10.1088/1757-899X/1279/1/012001

A.R. Puttige, K. Feng, W. Lu, T. Olofsson, "Are radiators ready for the challenges of the future: A review of advancements in radiators," E3S Web of Conferences, pp. 356, 2022. https://doi.org/10.1051/E3SCONF/202235603024

J. Li, J. Su, S. Wang, “Research on the Performance of Radiators in Hybrid Vehicle Thermal Management Systems,” World Electric Vehicle Journal, vol. 16, no. 2, 2025. https://doi.org/10.3390/WEVJ16020089

D. Dan, Y. Zhao, M. Wei, X. Wang, “Review of Thermal Management Technology for Electric Vehicles,” Energies, vol. 16, pp. 4693, 2023. https://doi.org/10.3390/EN16124693

C. Gong, J. Shen, Y. Yu, K. Wang, Z. Tu, “A novel radiator structure for enhanced heat transfer used in PEM fuel cell vehicle,” International Journal of Heat and Mass Transfer, vol. 157, pp. 1-7, 2020. https://doi.org/10.1016/J.IJHEATMASSTRANSFER.2020.119926

A.U. Yakubu, J. Zhao, Q. Jiang, X. Ye, J. Liu, Q. Yu, S. Xiong. “A comprehensive review of primary cooling techniques and thermal management strategies for polymer electrolyte membrane fuel cells PEMFC,” Heliyon, vol. 10, no. 19, pp. e38556, 2024. https://doi.org/10.1016/J.HELIYON.2024.E38556.

D.K. Madheswaran, A. Jayakumar, E.G. Varuvel, “Recent advancement on thermal management strategies in PEM fuel cell stack: a technical assessment from the context of fuel cell electric vehicle application,” Energy Sources, Part A: Recovery, Utilization, and Environmental Effects, vol. 44, no. 2, pp. 3100–3125, 2022. https://doi.org/10.1080/15567036.2022.2058122

F. Dika, M. Dagbasi, M. Adedeji, H. Adun, “Performance analysis of a wavy fin-and-tube automobile radiator operating on ethylene glycol and water based ternary nanofluids,” Heliyon, vol. 11, no. 1, pp. 1-18, 2025. https://doi.org/10.1016/j.heliyon.2024.e41509.

[13 8] M. Lipnicky, Z. Brodnianska, “The effect of a new approach to cooling the external heat exchange surfaces of a car cooler with air nozzles on the cooling process,” Appl. Sci., vol. 14, pp. 1-20. 2024. https:// doi.org/10.3390/app14062227

P. Bencs, M. Alktranee, “The potential of vehicle cooling systems,” in Proc. Journal of Physics: Conference series, 2021, pp. 1-11. https://doi.org/10.1088/1742-6596/1935/1/012012

T. Pacifique, W.J. Sohn, S.-B. Choi, “A novel active cooling system for internal combustion engine using shape memory alloy-based thermostat,” Sensors, vol. 24, no. 8, pp. 1-22, 2023. https://doi.org/10.3390/s23083972

S. Porgara, G. Huminic, A. Huminic, R. Najibolashrafic, S.S. Somayeh, “Application of nanofluids in heat exchangers - a state-of-the-art review,” Intl. J. Thermofluids, vol. 24, pp. 1-32, 2024. https://doi.org/10.1016/j.ijft.2024.100945

M.A. Rahman, S.M.M Hasnain, S. Pandey, A. Tapalova, N. Akylbekov, R. Zairov, “Review on nanofluids: preparation, properties, stability, and thermal performance augmentation in heat transfer applications,” ACS Omega, vol. 9, no. 30, pp. 32268 - 33302, 2024 https://doi.org/10.1021/acsomega.4c03279

Z.U. Zango, K.H. Ibnaouf, A. Garba, O. Aldaghri, I.A. Wadi, A. Hosseini-Bandegharaei, O. Baigenzhenov, “Advances in green synthesis, modification strategies, and photocatalytic application of metal oxide nanoparticles for organic pollutants degradation: A comprehensive and in-depth review,” J. Molecular Liquids, vol. 428, pp. 1-34, 2025. https://doi.org/10.1016/j.molliq.2025.127497.

S. Hashimoto, K. Yano, Y. Hirota, H. Uchiyama, S. Tsutsui, “Analysis of enhancement mechanism for thermal conductivity of nanofluids by inelastic X-ray scattering,” International Journal of Heat & Mass Transfer, vol. 173, pp. 1-8, 2021. https://doi.org/10.1016/j.ijheatmasstransfer.2021.121245

B. Anegbe, I.H. Ifijen, M. Maliki, “Graphene oxide synthesis and applications in emerging contaminant removal: a comprehensive review,” Environ. Sci. Eur., vol. 36, no. 15, pp. 1-34, 2024. https://doi.org/10.1186/s12302-023-00814-4

D. Malavekar, S. Bachankar, D. Pawar, A. Bagde, S. Patil, S. Khot, C.D. Lokhande, S. Sankapal, J.H. Kim, “Advancements in graphene and its derivatives based composite Materials: A comprehensive review on Synthesis, Characterization, and supercapacitive charge storage,” Chemical Engineering Journal, vol. 501, pp. 1-43, 2024. https://doi.org/10.1016/j.cej.2024.157533

S.Z. Haeri, M. Khiadani, B. Ramezanzadeh, H. Kariman, M. Zargar. “Photo-thermal conversion properties of hybrid NH2-MIL-125/TiN/EG nanofluids for solar energy harvesting,” Appl. Thermal Engineering, vol. 258, no. B, pp. 1-14, 2025. https://doi.org/10.1016/j.applthermaleng.2024.124607.

H. Ali, M.U. Sajid, “Thermal conductivity of hybrid nanofluids: a critical review,” Intl. J. Heat and Mass Transfer, vol. 126, no. A, pp. 1-24, 2018. https://doi.org/10.1016/j.ijheatmasstransfer.2018.05.021

X.-W Yi, Z. Zhang, Z.-W. Liao, X.-J. Dong, J.-Y. You, G. Su, “T-carbon: Experiments, properties, potential applications and derivatives,” Nano Today, vol. 42, pp. 101346, 2022. https://doi.org/10.1016/j.nantod.2021.101346.

J.D. Quadros, S.A. Khan, P.T.I Mogul, R. Hanumanthraya, M. Abbas, C.A. Saleel, S. Shaik, ”Heat transfer characteristics of fullerene and titania nanotube nanofluids under agitated quench conditions,” ACS Omega, vol. 7, pp. 47764 - 47783, 2022. https://doi.org/10.1021/acsomega.

B. Reding, M. Khayet, “Thermal conductivity and thermal diffusivity of fullerene-based nanofluids,” Sci Rep., vol. 12, pp. 1-13, 2022. https://doi.org/10.1038/s41598-022-14204-y

X. Li, W. Chen, C. Zou, “The stability, viscosity and thermal conductivity of carbon nanotubes nanofluids with high particle concentration: A surface modification approach,” Powder Technology, vol. 361, pp. 957-967, 2020. https://doi.org/10.1016/j.powtec.2019.10.106.

Khoswan, H. Nassar, M. Assali, A. AbuSafa, S. Sawalha, H.S. Hilal, “Why carbon nanotubes improve aqueous nanofluid thermal conductivity: a qualitative model critical review” Processes, vol. 12, pp. 834, 2024. https://doi.org/10.3390/ pr12040834

K. Elsaida, M.A. Abdelkareem, H.M. Maghrabiee, E.T. Sayed, T. Wilberforcef, A. Baroutajig, A.G. Olabi, “Thermophysical properties of graphene-based nanofluids,” International Journal of Thermofluids, vol. 10, pp. 1-12, 2021. https://doi.org/10.1016/j.ijft.2021.100073

A. Yusuf, M.M. Bhatti, C.M. Khalique, “Computational study of the thermophysical properties of graphene oxide/vacuum residue nanofluids for enhanced oil recovery,” J. Therm Anal Calorim., vol. 150, pp. 771–783, 2025. https://doi.org/10.1007/s10973-024-13921-y

R. Hoffmann, A.A. Kabanov, A.A. Golov, D.M. Proserpio, “Homocitans and carbon allotropes: for an ethics of citation,” Angew. Chem. Int. Ed., vol. 55: pp. 10962 -10976, 2016. https://doi.org/10.1002/ange_201600655

M. Bahiraei, S. Heshmatian, “Electronics cooling with nanofluids: A critical review. Energy Conversion and Management,” vol. 172, pp. 438 - 456, 2018. https://doi.org/10.1016/j.enconman.2018.07.047

G. Sharma, V. Khullar, S. Soni, “Thermophysical and photothermal characteristics of surfactant free graphene oxide, functionalized graphene oxide and reduced graphene oxide nanofluids,” J. Material Science and Technology, vol. 0, pp. 1-13, 2024. https://doi.org/10.1177/02670836241274637

G. Bharadwaj, K. Sharma, A.K. Pandey, “Thermal conductivity augmentation of reduced graphene oxide-based nanofluids and its solar application,” MRS Advances, vol. 9, pp. 1004–1010, 2024. https://doi.org/10.1557/s43580-024-00828-x

M. Hadadian, E.K. Goharshadi, A. Youssefi, “Electrical conductivity, thermal conductivity, and rheological properties of graphene oxide-based nanofluids,” J. Nanopart. Res., 16: 1-17, 2014. https://doi.org/10.1007/s11051-014-2788-1

D. Cabaleiro, P. Estelle, H. Navas, A. Desforges, B. Vigolo, “Dynamic viscosity and surface tension of stable graphene oxide and reduced graphene oxide aqueous nanofluids,” J. Nanofluids, vol. 7, pp. 1081–1088, 2018. https://doi.org/10.1166/jon.2018.1539

R. Ranjbarzadeh, A.H. Meghdadi Isfahani, M. Afrand, A. Karimipour, M. Hojaji, “An experimental study on heat transfer and pressure drop of water/graphene oxide nanofluid in a copper tube under air cross-flow: Applicable as a heat exchanger,” Appl. Therm. Eng., vol. 125, pp. 69 – 79, 2017. https://doi.org/10.1016/j.applthermaleng.2017.06.110

M.J. Bai, J.L. Liu, J. He, W.J. Li, J.J. Wei, L.X. Chen, J.Y. Miao, C.M. Li, “Heat transfer and mechanical friction reduction properties of graphene oxide nanofluids,” Diam. Relat. Mater., vol. 108, pp. 107982, 2020. https://doi.org/10.1016/j.diamond.2020.107982

Kazemi, M. Sefid, M. Afrand, “Improving the thermal conductivity of water by adding mono & hybrid nano-additives containing graphene and silica: A comparative experimental study,” Intl. Communications in Heat and Mass Transf., vol. 116, pp. 1-13, 2020. https://doi.org/10.1016/j.icheatmasstransfer.2020.104648

B.R. Ponangi, , V. Krishna, K.N. Seetharamu, “Effect of Ultralow Concentrated Reduced Graphene Oxide Nanofluid on Radiator Performance,” Journal of Heat Transfer, vol. 143, no. 8, 2021. https://doi.org/10.1115/1.4051233

R.H. Ong, W.M.E. Iskandar, M. Yapp Joo, M.M.R. Khan, M.K. Anuar Mohamed. “Effects of natural-based SiO2 nanocoolant on car radiator: Thermal profile,” Materials Today: Proceedings, vol. 66, pp. 2734–2737, 2022. https://doi.org/10.1016/J.MATPR.2022.06.505

Joshi, V. Khatawate, N.R. Banapurmath, R.P. Shankara, A.M. Sajjan, T.M.Y. Khan, N.H. Ayachit, I.A. Badruddin, “Experimental and numerical investigation of heat transfer characteristics of radiator using Graphene Amine-based nano coolant,” Case Studies in Thermal Engineering, vol. 63, pp. 105389, 2024. https://doi.org/10.1016/J.CSITE.2024.105389

U.S. Behera, J.S. Sangwai, H.-S. Byun, "A comprehensive review on the recent advances in applications of nanofluids for effective utilization of renewable energy,” Renewable and Sustainable Energy Reviews, vol. 207, pp. 1-28, 2025. https://doi.org/10.1016/j.rser.2024.114901.

M.M. Abady, D.M. Mohammed, T.N. Soliman, "Sustainable synthesis of nanomaterials using different renewable sources," Bull Natl Res Cent., vol. 49, no. 24, pp. 1-28, 2025. https://doi.org/10.1186/s42269-025-01316-4

Mahian , E. Bellos , C.N. Markides, R.A. Taylor, A. Alagumalai, L. Yang, C. Qin, B.J. Lee, G. Ahmadi, M.R. Safaei, S. Wongwises, "Recent advances in using nanofluids in renewable energy systems and the environmental implications of their uptake," Nano Energy, vol. 86, pp.106069, 2021, https://doi.org/10.1016/j.nanoen.2021.106069.

N.K. Cakmak (2020), “The impact of surfactants on the stability and thermal conductivity of graphene oxide de-ionized water nanofluids,” J. of Thermal Analysis and Calorimetry, vol. 139, pp. 1895–1902, 2020. 10.1007/s10973-019-09096-6.

Kaggwa, M. Atkins, A. Tarighaleslami, "Thermal Performance of Selected Nanofluids with Surfactants," Int J Thermophys, vol. 44, pp. 1-15 160, (2023). https://doi.org/10.1007/s10765-023-03271-6

J. Wang, G. Li, T. Li, M. Zeng, B. Sunden, "Effect of various surfactants on stability and thermophysical properties of nanofluids," Journal of Thermal Analysis and Calorimetry, vol. 143, pp. 4057–4070, 2021. https://doi.org/10.1007/s10973-020-09381-9

Shamsuddin H.S., Estelle P., Navas J., Ghazali N.M., M. Mohamad, "Effects of surfactant and nanofluid on the performance and optimization of a microchannel heat sink," Intl. Journal of Heat and Mass Transfer, vol. 175, pp. 1-34, 2021. https://doi.org/10.1016/j.ijheatmasstransfer.2021.121336.

R.J. Moffat, “Describing the uncertainties in experimental results. experimental thermal and fluid science,” vol. 1, pp. 3 - 17, 1988. https://doi.org/10.1016/0894-1777(88)90043-X